Kathrein, C., Bai, W., Nunns, A., Gwyther, J., Manners, I., Boeker, A., ... Ross, C. (2016). Electric field manipulated nanopatterns in thin films of metalorganic 3-miktoarm star terpolymers. Soft Matter (The Royal Society of Chemistry), 12, 4866-4874. DOI: 10.1039/C6SM00451B

Journal Name

ARTICLE TYPE

Cite this: DOI: 10.1039/xxxxxxxxxx

Electric Field induced Morphological Transitions in Thin Films of Metalorganic 3-Miktoarm Star Terpolymers†

Christine C. Kathrein,[a] Wubin Bai,[b] Adam Nunns,[c] Jessica Gwyther,[c] Ian Manners,[c] Alexander Böker,[d] Larisa Tsarkova,[a] and Caroline A. Ross*[b]

Received Date
Accepted Date

DOI: 10.1039/xxxxxxxxxx

www.rsc.org/journalname

We report the effect of electric field on the morphological transitions and ordering behavior of polyferrocenylethylmethylsilane block (PFEMS)-containing copolymers. By analyzing structures in swollen films of metalorganic sphere- and cylinder-forming diblock copolymers, as well as of 3-miktoarm polyisoprene-arm-polystyrene-arm-PFEMS (3μ-ISF) terpolymers, we decouple two types of responses to the electric field: an increase in the volume fraction of the PFEMS block by oxidation of the ferrocenyl groups inducing morphological transformation, and orientation of the dielectric interfaces of microdomains parallel to the electric field vector. In the case of 3μ-ISF, the former effect dominates the morphological behavior at high electric field strengths, leading to a well-ordered hexagonal dot pattern. Our results demonstrate multiple tunability of ordered microdomain morphologies, suggesting future applications in nanofabrication and surface patterning.

1 Introduction

Star-shaped 3-miktoarm triblock terpolymers (3μ-ABC) exhibit an extraordinary structural diversity and thin films of these materials are of interest in nanofabrication and nanolithography. In contrast to linear ABC terpolymers, the three blocks of a 3μ-ABC polymer are connected at a single junction point. In the microphase-separated structure the junction points tend to assemble along linear or curved trajectories defining the vertex between the three microdomains[1]. Such geometrical constraint together with the minimization of unfavorable contacts between incompatible blocks gives rise to novel morphologies not observed for linear triblock terpolymers.

Simulations[2], bulk-[3] and thin film studies[4] of different 3μ-ABCs revealed a large variety of structures such as several Archimedean tilings[5–7] composed of coaxial prisms including the space groups c2mm, p3m1, p4mm, p6mm, and p4gm. Also, three-colored honeycomb structures were observed provided that the interaction parameters and volume fractions of the three components are of about equal value[8,9]. Strongly differing χ parameters were found to result in partial mixing of blocks minimizing the contact area between the constituents with the energetically most unfavorable interaction parameter[10,11]. Key parameters determining the morphology are the block lengths, the selectivity of solvents used for annealing, segment-segment interaction parameters, as well as chain deformation energies[10], and in the case of thin films, surface and interface energies are also important. The annealing conditions, for example variations in composition and vapor pressure of solvents, also affect the resulting morphologies.[4] Further, specific functionalities of the blocks contribute to the hierarchical complexity of the nanostructures.

Polymers comprising polyferrocenylsilane (PFS) blocks represent an interesting class of materials since they combine the structural diversity of multiblock polymers with the unique physical properties of the PFS block, such as electroactivity and electrochromism which arise from the presence of transition metals in the polymer backbone.[12,13] These materials can be used as precursors for magnetic materials by oxidation or pyrolysis.[14–17] Upon iodine doping, PFS has also been shown to exhibit p-type conductivity.[18] Prior work showed that 3-miktoarm star terpolymers of polyisoprene-*arm*-polystyrene-*arm*-poly(ferrocenylethylmethylsilane) (3μ-ISF) form a variety of different thin film microstructures, influenced by the film thickness and by the partial pressure of chloroform vapor in the annealing chamber, which controls the swelling and relative volume fraction of the polyiso-

[a] *DWI - Leibniz Institut für Interaktive Materialien, Institut für Physikalische Chemie, RWTH Aachen University D-52062 Aachen, Germany*
[b] *Department of Materials Science and Engineering, Massachusetts Institute of Technology, 77 Massachusetts Avenue, Cambridge, Massachusetts 02139, United States, Fax: XX XXXX XXXX; Tel: XX XXXX XXXX; E-mail: caross@mit.edu*
[c] *School of Chemistry, University of Bristol, Bristol BS8 1TS, United Kingdom*
[d] *Lehrstuhl für Polymermaterialien und Polymertechnologien, Fraunhofer-Institut für Angewandte Polymerforschung - IAP, University of Potsdam, D-14476 Potsdam-Golm, Germany*
* corresponding author

prene block.[4] This illustrates that small changes in the effective volume fraction can alter the thin film structure.

Previously electric fields have been shown to induce ordering and phase transitions in thin film and bulk diblock copolymers. The basic concept determining the behavior of *non-metal-containing* block copolymers in electric fields is the unfavorable electrostatic energy of block-block interfaces oriented perpendicular to the electric field vector ($\vec{E}$) with respect to those aligned parallel to $\vec{E}$. Electric-field-induced ordering and defect annihilation have been thoroughly investigated since the work of Amundson et al. in 1991.[19–28] Reorientation of dielectric interfaces parallel to the electric field vector is the anticipated response when a certain threshold voltage, dependent on the polymer and annealing conditions, is exceeded.

Polyferrocenylethylmethylsilane (PFEMS) block-containing copolymers are expected to have a notable response to an electric field due to the iron atoms complexed inside the microdomains, similar to the reported enhanced ordering effect of LiCl salt added to polystyrene-*block*-poly methyl methacrylate diblock copolymer.[25]. Earlier studies describe the influence of electrochemical oxidation and applied voltage on the electroactive PFS block. In both cases an oxidation of the ferrocenyl groups is induced which affects the PFS volume.[29] Electrochemical oxidation was analyzed by Shi et al. who observed a more than 70 % increase in the Kuhn segment length of poly(ferrocenylmethyl(phenyl)silane) and poly(ferrocenyl dimethyl silane) polymers upon electrochemical oxidation of the ferrocenyl groups[30]. Due to the electrostatic interactions between positive charged segments a stretched conformation of chains is favored to maximize the distance between like charges[31]. Analyzing the effects of voltage, Li et al. measured a widening of PFS cylinders by up to 100 % in a cylinder-forming polystyrene-*block*-poly(ferrocenylethylmethylsilane) (PFEMS-*b*-PS) block copolymer with conductive probe atomic force microscopy upon application of a negative voltage bias between -4 V and -9 V[15]. The electric field strength is therefore envisaged to be an additional control parameter determining the thin film morphology.

In this paper we report the effect of the electric field on the morphological development and ordering of nanostructures in swollen thin films of diblock copolymers and 3-miktoarm star terpolymers containing a functional PFEMS block. The ordering and morphological behavior of the diblock copolymers exhibit two effects of an electric field: an increase in the volume fraction of the PFEMS block by oxidation of the ferrocenyl groups leading to a morphological transformation, and orientation of the dielectric interfaces parallel to $\vec{E}$. Microdomains of 3-miktoarm star terpolymers exhibit ordering and a sequence of phase transitions with increasing electric field strength. At moderate field strengths the observed phase transitions can be attributed to the electrostatic energy penalty associated with dielectric interfaces not aligned parallel to $\vec{E}$.[20–28] At higher electric field strengths the electroactive response of the PFEMS block becomes the dominant factor determining the morphological transition. Such dual responsive behavior facilitates structural switchability and provides a high degree of ordering upon application of electric field stimuli.

2 Experimental

2.1 Polymers

PS-*b*-PFEMS sphere- and lamellae forming polymers were synthesized as described earlier[32]. The sphere-forming diblock copolymer had a molecular weight of 100 kg/mol and a volume fraction of PFEMS of 16%, while the lamellae-forming PS-*b*-PFEMS had a volume fraction of PFEMS of 43 % and a molecular weight of 58 kg/mol (PDI=1.04). The later was blended with polystyrene homopolymer (homo-PS) (7.7 kg/mol, PDI=1.1) to obtain a cylindrical morphology. The volume fraction of homo-PS was 17 wt%.

The 3-miktoarm star terpolymers were synthesized according to Nunns et al.[33] A 3-miktoarm star terpolymer with a composition of 39 vol% of polyisoprene, 35 vol% of polystyrene and 26 vol% of poly(ferrocenylethylmethylsilane) was utilized in which the individual blocks had molecular weights of 23 kg/mol, 22.5 kg/mol and 20.5 kg/mol, respectively. To promote the formation of ordered microdomains, 15 wt% of homo-PS with a molecular weight of 12.5 kg/mol and a PDI of 1.04 was added to the copolymer.[4].

2.2 Thin Film preparation

Thin films of the sphere-forming polystyrene-*block*-polyferrocenylethylmethylsilane (PS-*b*-PFEMS) were spin coated for 30 s at 4000 revolutions per minute (rpm) from 2 wt% solutions in toluene. The initial film thickness prior to solvent vapor annealing was 50 nm. 2 wt% solutions of the cylinder forming PS-*b*-PFEMS/homo-PS blend in toluene were prepared by spin coating at 3000 rpm for 30 s yielding an initial film thickness of 50 nm. 45 nm thick films of the 3μ-ISF/homo-PS blend were obtained by spin coating from a 1.5 wt% solution of the polymer in toluene at 3000 rpm for 30 s.

2.3 Solvent Vapor Annealing

The thin films exhibited swelling ratios ($SR = \frac{h_{swollenfilm}}{h_{unswollenfilm}}$) of $1.7-1.8$ upon exposure to a continous flow of chloroform vapor produced by bubbling N_2 gas through a $CHCl_3$ reservoir and directing the vapor through the solvent vapor annealing chamber. Swelling ratios were controlled by adding a separate stream of N_2. The annealing chamber had a volume of 353.4 cm^3. A quartz lid was tightly screwed to the top of the chamber which allowed the measurement of the swelling ratio via a Filmmetrics F20-UV spectral reflectometer during the experiment. The thin films were exposed to the solvent vapor for two hours and were then quenched within 1 s by removing the lid of the chamber.

2.4 Electric Field

Experiments were conducted on oxidized silicon wafers and on glass slides with two gold electrodes, each 0.5 cm $\times$ 0.5 cm and 100 nm thick. Experiments at fixed electric field were performed on samples with gold electrodes separated by a 40 μm wide gap. An electric field of 10 V/μm was applied between the electrodes during solvent vapor annealing.

To vary the electric field strength within a single experiment, substrates with a stepwise varying gap size between 9.3 μm and

78 μm were utilized as schematically shown in Figure 2 (b). This led to electric field strengths between 1.9 V/μm and 16 V/μm when a voltage of 150 V was applied between the two gold electrodes. This assured comparable conditions of film thickness and swelling ratio during solvent vapor annealing leaving the electric field strength as the only variable.

2.5 Imaging

Prior to imaging the thin films were exposed to O_2 plasma for 12 s which selectively removed the PI and PS domains and oxidized the PFEMS domains. AFM measurements were performed with a Nanoscope IV from Bruker using a super fine probe (μmash HiRES-W/8/A/BS, 75 kHz, 3.5 Nm). An Orion He-Ion microscope from Zeiss was used to image samples coated with a 2 nm thick layer of sputtered Au. To stain the samples after annealing, the thin films were placed in a chamber with an aqueous solution of OsO_4 (4 wt%) for 4 h. OsO_4 selectively binds to the PI domains increasing its contrast in the He-Ion images.

3 Results and discussion

Thin films of a cylinder and a sphere forming PS-*b*-PFEMS block copolymer or blend, as well as of a 3-miktoarm star terpolymer with PS, PI and PFEMS blocks were analyzed after solvent vapor annealing in chloroform, with and without an applied electric field.

3.1 PS-*b*-PFEMS Diblock Copolymers under Application of an Electric Field

(i) Sphere-forming PS-*b*-PFEMS Diblock Copolymers.

In the following we will elucidate how the iron containing moiety present in the PFEMS block alters the behavior of the polymer when exposed to electric fields compared to non-metal containing block copolymers. The results of this section are crucial for the interpretation of the effect electric fields have on the mictoarm star terpolymers.

Figure 1 (a) displays a 50 nm thin film of a 100 kg/mol PS-*b*-PFEMS block copolymer with a volume fraction of PFEMS of 16% solvent vapor annealed in $CHCl_3$ vapor for 2 h. After removal of the PS matrix via an O_2 plasma etch, AFM analysis reveals poorly ordered PFEMS spheres with diameter of 43 nm $\pm$ 2 nm. In contrast, Figure 1 (b) displays a film that was solvent vapor annealed under the same conditions but including an electric field of 10 V/μm. Close packed spheres coexist with regions of striped patterns (in-plane cylinders) with random orientations relative to the direction of the electric field. Considering that the film thickness is sufficient to accommodate only a monolayer of in-plane cylinders, we believe the close packed features are spheres rather than vertical cylinders. Furthermore, vertical cylinder formation is unlikely to be induced by the electric field because this maximizes unfavorable dielectric interfaces perpendicular to $\vec{E}$. This morphological behavior suggests that on the one hand, the electric field induces ordering of the spherical morphology, and on the other hand, promotes an order-order phase transition from spheres to cylinders.

The observed ordering of spheres is unexpected since it does not lead to a reduction of dielectric interfaces perpendicular to $\vec{E}$, which is the driving force responsible for the realignment of lamellae and cylindrical block copolymer morphologies exposed to electric fields. It is known that in bcc or gyroid morphologies, frustration occurs independent of the orientation of the microdomains with respect to $\vec{E}$.[34,35] In these cases, electric fields induce phase transitions into uniaxial structures when the composition of the block copolymer is near a phase boundary.[34] Xu et al. demonstrated that the improvement of the long-range order in a bcc phase of a non-metal-containing block copolymer upon application of electric fields can only be accomplished by first inducing an order-order phase transition from spheres into a cylindrical microdomain structure which is aligned by the electric field, and by subsequent reformation of the bcc structure.[35] This stands in clear contrast to the results of our experiments which show that improved ordering can be achieved in bcc forming thin films of PS-*b*-PFEMS without requiring a prior phase transition into an uniaxial phase. We therefore conclude that the improved

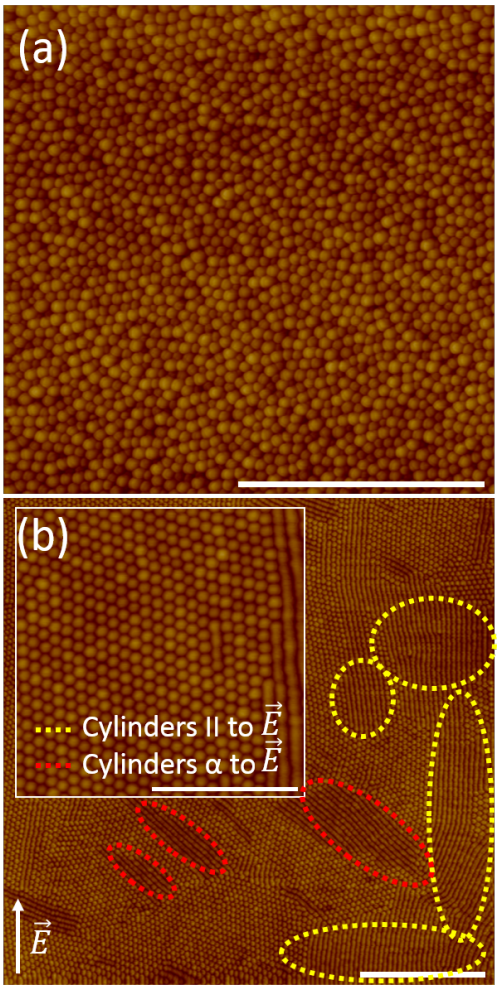

Fig. 1 AFM height images of sphere-forming PS-*b*-PFEMS block copolymer thin films after solvent vapor annealing in $CHCl_3$, (a) without and (b) with application of an in-plane electric field of 10 V/μm. The electric field induces ordering as well as a sphere-to-cylinder transition. Cylinders parallel to $\vec{E}$ are marked with a yellow dashed line while those at angles to $\vec{E}$ are indicated by a red dashed line.

order may be related to polarization of the iron-containing PFEMS spheres, which is specific for block copolymers with a metal-containing minority block. Furthermore, in case of non-metal containing block copolymers cylinders induced from spheres by application of electric field form with their long axis parallel to the electric field vector. This again stands in contrast to our experiments where only about half of the striped domains are oriented along the direction of the electric field, while the long axis of the other half is directed at different angles to $\vec{E}$. This implies that the reduction of the fraction of the electrostatically unfavorable interfaces oriented perpendicular to the electric field vector cannot be the overriding factor determining the cylinder formation.

A possible explanation for the behavior can be found in literature: Electrochemical oxidation[30] as well as application of voltage[15] have been reported to alter the microstructure of PFEMS-containing block copolymers due to the effective increase of the volume fraction of the electroactive PFEMS block. As an example, Peter et al. reported electrochemically induced volume and morphology changes in surface grafted PFS layers upon applying voltages between 400 mV and 600 mV.[36] The change of volume in these redox-active monolayers was attributed to a reversible oxidation increasing the charge density in the polymer backbone. It was postulated that the increased charge density attracts additional counter-ions as well as solvent molecules, resulting in an overall increase of the layer thickness. Considering the results described above, the observed sphere to cylinder transition is more likely a thermodynamically driven phase transition induced by an effective increase of the volume fraction of the PFEMS block. Unlike the kinetically-driven transformation observed in the case of non-metal containing block copolymers this explains the formation of cylinders at different angles to $\vec{E}$. The additional charges associated with the oxidation of the ferrocenyl groups induced by the high voltage might increase the selective solvent uptake of the PFEMS block resulting in an enhanced PFEMS volume fraction and therefore a sphere to cylinder phase transition. The electric field would further enhance the polarity difference between polar PFEMS and non-polar PS, increasing chloroform solubility in PFEMS.[37,38] The change in solvent solubility of the PFS block through oxidation of the ferrocene moieties of PS-*b*-PFS copolymers has furthermore been reported by Eloi et al.[39]

(ii) Cylinder forming PS-*b*-PFEMS Diblock Copolymer Blends. To confirm the assumption that the applied voltage leads to an oxidation of the ferrocenyl groups and hence an increase in PFEMS volume fraction thin films of a cylinder forming block copolymer blend were analyzed at various electric field strengths. To validate the assumption an increase in cylinder width with increasing electric field strength is anticipated. The thin films of the cylinder-forming PS-*b*-PFEMS blend were prepared by adding polystyrene homopolymer to a lamellae- forming PS-*b*-PFEMS block copolymer. The unblended diblock copolymer exhibits an in-plane lamellar morphology. Figure 2 (b) shows a schematic of the substrate utilized for our experiments. It comprises two gold electrodes separated by a gap of varying thickness. This allows the analysis of the effect of different field strengths on a single sample assuring comparable annealing conditions. As shown in the close up image in Figure 2 (a) the thinnest and thickest gap i.e. the highest and lowest field strength are adjacent to one another allowing direct comparison of the film thickness at different field strengths under the light microscope.

Figure 2 (c) and (d) display He-Ion images of surface structures in 50 nm thick films of PS-*b*-PFEMS/homo-polystyrene (homo-PS) blend upon 3 h of annealing in chloroform vapor. Cylinders in Figure 2 (c) were exposed to an electric field strength of 1.7 V/μm during solvent vapor annealing while an electric field of 10.9 V/μm was applied to the cylinders in Figure 2 (d). The difference in PFEMS cylinder width at different field strengths can already be seen by eye in the He-Ion images.

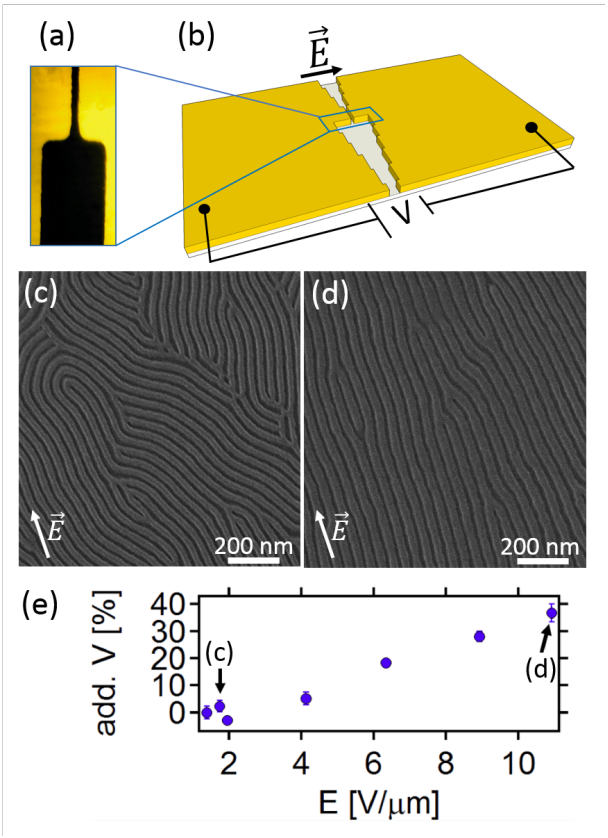

Fig. 2 (a) Close up image of the gap between two gold electrodes where the thinnest and thickest part of the gap are adjacent to one another. (b) Schematic image of the substrates. (c, d) He-Ion images of the cylinder forming PS-*b*-PFEMS/homo-PS blend after solvent vapor annealing under application of an electric field of (c) 1.7 V/μm and (d)10.9 V/μm. The oxidized PFEMS block appears light gray, and the dark gray regions correspond to the removed PS block. (e) Graph showing the increase in PFEMS cylinder volume in % vs the applied electric field strength in V/μm.

In Figure 2 (e) the increase in PFEMS volume is plotted against the electric field strength. The cylinder widths were measured from He-Ion microscope images via Image J software. For each field strength the average width was measured from five areas of three different images each. The increase in cylinder volume was calculated according to $V_{add.}[\%] = (\frac{{r_2}^2}{{r_1}^2} \times 100) - 100$, in which r_1 is the PFEMS cylinder radius at zero electric field while r_2 is the radius measured at the respective electric field strength. Exemplary He-Ion images corresponding to the field strengths 1.7 V/μm and

10.9 V/μm are displayed in Figure 2 (d,e). The results clearly show an increase in cylinder width with electric field strength when a threshold voltage of 2 V/μm is exceeded. This is further evidence for an electroactive response induced by the high voltage partially leading to an oxidation from Fe(II) to Fe(III). The positive charges along the polymer backbone promote a stretched polymer chain conformation increasing the distance between like-charged segments. Considering the dipole moment of chloroform it is assumed that the increased positive charge in the polymer backbone enhances the selective solvent uptake of chloroform by the PFEMS block compared to the unoxidized polymer[36]. This results in an increase in the volume fraction of the electroactive PFEMS block as previously also described in other studies.[15,29] In our case the highest applied field strength led to an increase by about 37 %, significantly less than the up to 100 % widening measured with conductive probe atomic force microscopy in cylinder forming PFEMS-*b*-PS block copolymer upon application of a negative voltage bias between -4 V and -9 V[15]. This implies that only parts of the ferrocenyl groups were oxidized.[31] For block copolymers such as polystyrene-*block*-poly(methyl methacrylate) or polystyrene-*block*-polyisoprene which are solely composed of organic blocks no alteration in volume fraction is anticipated upon application of electric field.

The results reveal that the electric field has a profound effect on the ordering and phase transitions of PS-*b*-PFEMS block copolymers. This is due to two factors: an increase in the volume fraction of the PFEMS block by oxidation of the ferrocenyl groups which can drive a morphological transformation, and the anticipated orientation of the dielectric interfaces to lie parallel to $\vec{E}$. We now show how these factors affect the microphase separation of 3-miktoarm star terpolymers of PS, PI and PFEMS.

3.2 Surface structures in solvent-annealed films of 3μ-ISF/homo-PS blends

Surface structures of the 3μ-ISF/homo-PS blend in 45 nm thick films were analyzed after annealing in chloroform vapor and compared to those subjected to electric field of varying strength during solvent vapor annealing. In the following the thin film structure without application of electric field will be described.

The analysis and identification of the thin film structure can be complicated by surface fields, i.e. the difference in interfacial energies between the block copolymer constituents at the film surface[41,42], which may lead to a distortion of a unit cell[43,44], as well as redistribution of the blocks at film interfaces, inducing non-bulk morphologies[45]. A further variable is introduced by the addition of PS homopolymer which enhances chain relaxation. Without the addition of this compatibilizer the equilibrium structure of 3μ-ISF in thin films is lamellar, with the majority PI block segregated to the free surface due to its low surface tension, while the two other blocks form the bottom layer of the lamella.

Surface structures in blended 3μ-ISF films are shown in Figure 3 (a,b) where (b) is higher magnification. (a1,b1) are height and (a2,b2) are phase images. Prior to imaging, an O_2 plasma etch was applied to remove the top wetting layer of the soft PI block in order to reveal underlying microphase-separated structures. The plasma etches away the PI domains faster than the PS domains[4], and simultaneously oxidizes the PFEMS block. As shown in Figure 3 (a1), the 3μ-ISF copolymer assembles into alternating stripes and dot-like structures, which appear as two types of spheres (marked as A and B structures) in the close-up images in Figure 3 (b1, b2). While A-type structures appear as higher (brighter) cylinders in the height images (b1), the phase images (b2) reveal soft (dark) shells around a hard core, where the core is most likely made of the oxidized PFEMS block. In contrast, in B-type spheres the hard core is surrounded by two shells: a thin layer of harder shell formed, presumably, by PS homopolymer and an outer dark (soft) PI shell. The two types of structures also differ in their shapes, with type B having a spherical morphology, and type A spheres having a distorted anisotropic shape, making them directionally assembled into cylinders.

Considering the room temperature χ parameters $\chi_{\text{PFEMS-}b\text{-PS}} \sim 0.08 < \chi_{\text{PI-}b\text{-PS}} \sim 0.1 < \chi_{\text{PI-}b\text{-PFEMS}} \sim 0.17$[4], and the fact that the degree of polymerization (N) of the three blocks is of about equal value, it becomes apparent that the contact between PI and PFEMS is energetically most unfavorable. Therefore, the contact area between PFEMS and PI is minimized by the formation of a PS shell surrounding the PFEMS microdomains. This requires partial mixing of the PS and PI domains[10] as schematically demonstrated in Figure 3 (d) since the three blocks are connected at a single junction point. A schematic illustration of the proposed structure is given in Figure 3 (d). A possible reason for the formation of two different types of spheres could be the addition of PS homopolymer. Yamauchi et al. found that the addition of poly(dimethylsiloxane) homopolymer to a 3 miktoarm star terpolymer of polyisoprene-*arm*-polystyrene-*arm*-poly(dimethylsiloxane) led to defects through irregular distribution of the homopolymer throughout the microdomain structure.[1] Therefore, we conclude that the homo-PS is selectively adsorbed to every second row of spheres (B) forming a thicker PS shell around them which allows a wider spacing between the spheres and a non-distorted spherical morphology. The close packing and deformation of the spheres (A) agglomerated into cylindrical structures can be attributed to the strong tendency of the polymer to decrease the unfavorable PI/PFEMS contact under these annealing conditions. Furthermore, the formation of two different types of spheres underlines that the volume ratios between the blocks are not ideal for single pattern formation but are intermediate to two different structures[1].

Figure 3 (c) shows a He-Ion image of the sample. Prior to imaging the PI domains were selectively stained with OsO_4. The mean dimensions of the structures were measured via image J software and displayed as insets in Figure 3 (c). The PFEMS domains appear light gray in the He-Ion images while the PI and PS phases are darker gray and hard to distinguish.

3.3 Effect of electric field strength on the thin film structure of 3μ-ISF/homo-PS

To analyze the effect of the electric field on the thin film structure, 45 nm thick films of the 3μ-ISF/homo-PS blend were spin coated on substrates with a stepwise varying gap size between the

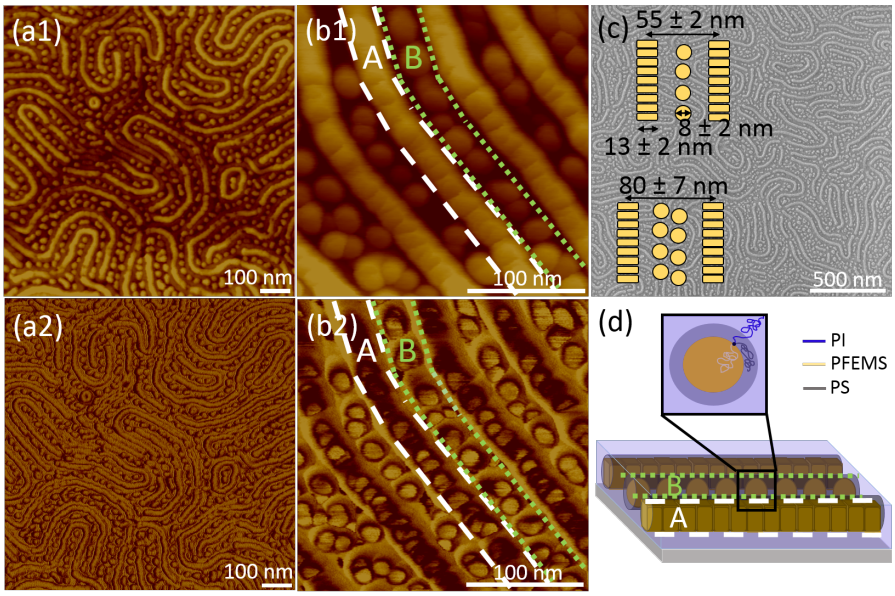

Fig. 3 AFM height (a1, b1) and phase (a2, b2) images of the 3μ-ISF/homo-PS blend after solvent vapor annealing in chloroform for 3 h. A and B mark the two different types of spheres. (c) He-Ion image of the same sample. (d) Schematic of the observed structure formed through partial mixing of the PI and the PS block.

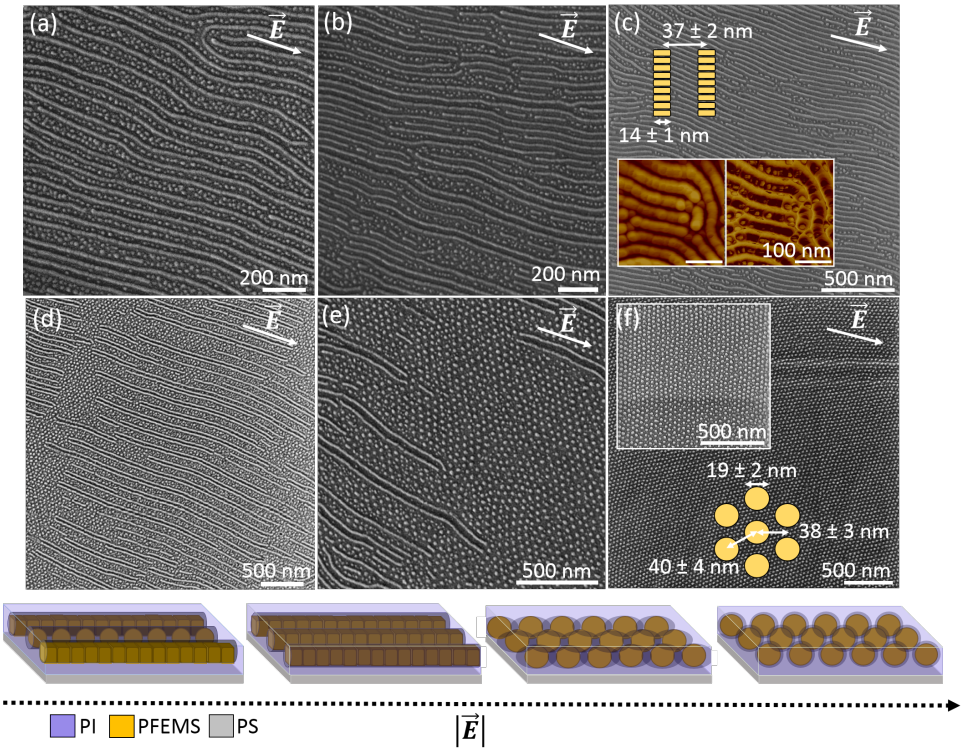

Fig. 4 He-Ion microscope images of the 3μ-ISF/homo-PS blend after solvent vapor annealing for 3 h at an electric field strength of (a) 2.0 V/μm, (b) 2.4 V/μm, (c) 2.7 V/μm, (d) 3.2 V/μm, (e) 3.9 V/μm and (f) 4.8 V/μm. The dimensions of the structures were measured from the He-Ion images and are indicated in the schematics in the images displaying the PFEMS block. The inset in (a) shows the AFM height and phase images of the structure measured with an ultrafine probe. Below the image a schematic of the proposed structural evolution upon application of $\vec{E}$ is given.

two gold electrodes, so that the electric field strength was varied between 2.0 V/μm and 16.0 V/μm in a single film. Choi et al.[40] previously reported that the film thickness can have a major influence on the thin film morphology of miktoarm star terpolymers. To exclude differences in film thickness from spin-coating, dewetting or terracing, the thin films within the gap were monitored via optical microscopy. Since regions of very high and very low field strength were directly adjacent to one another the direct compar-

ison of film thickness via optical microscopy was straight forward. A schematic image of the sample is given in Figure 2.

The structural evolution with increasing electric field is displayed in the He-Ion images in Figure 4 and may be compared to the structure annealed in zero field (Figure 3). A schematic of the structures is given underneath the images. The dimensions of the pattern features were measured via image J software and are indicated in the images. The transition from one structure to the next does not occur suddenly. At medium field strengths the different structures coexist which also supports the assumption that the structural evolution is not caused through different terracing conditions upon altering the field strength.

At moderate electric field strengths the cylinders of micellar aggregates start aligning in direction of the electric field vector, decreasing the area of PI/PS and PS/PFEMS interfaces perpendicular to $\vec{E}$ (Figure 4 (a)). The area of perpendicular interfaces is even further minimized when the spherical type-B spheres deform into type-A spheres with further assembly into a cylindrical aggregate at higher $|\vec{E}|$ as displayed in Figure 4 (b, c). The AFM height and phase image in the inset of Figure 4 (c) show that the structure still comprises tightly connected type-A spheres. Up to this point the behavior can be explained as the anticipated response of a copolymer upon exposure to an electric field.

Further increase of $|\vec{E}|$ results in a second phase transformation into well-ordered spherical domains (type-C spheres) as displayed in Figure 4 (d-f). A schematic of the structural evolution with increasing electric field strength is displayed in the bottom of Figure 4. On first sight this second phase transition seems counterintuitive since the portion of interfaces perpendicular to $\vec{E}$ is again increased. This can be explained when considering the results obtained from the diblock copolymers of PFEMS-*b*-PS under application of an electric field. The dominant driving forces inducing the phase transition from B-type into C-type spheres are the increase in PFEMS volume fraction due to the electroactive response of the PFEMS block. The additional positive charge increases the selective solvent uptake of the PFEMS block and forces the polymer to maximize the distance between like-charged segments thus resulting in a micellar arrangement with an average center to center distance of 40 nm. As previously demonstrated by Aissou et al., small changes in the relative volume fractions of the blocks greatly influence the thin film morphology[4]. While the relative amount of PI can be altered by controlling the swelling degree, the volume fraction of PFEMS can selectively be tuned by the electric field strength applied to the thin film structure.

4 Conclusions

This paper reports the first analysis of the effect of electric fields on the structure formation in 3-miktoarm star terpolymer thin films with PI, PS and PFEMS blocks blended with homo-PS, as well as the effect of electric field on sphere- and cylinder forming diblock copolymers and blends. In the diblock copolymers, electric field increased the volume fraction of PFEMS, drove a sphere-cylinder transition, and led to alignment of cylinders. In the star terpolymer blend, the solvent-annealed film consisted of two types of spheres. Electric field drove two different phase transitions. At moderate electric fields, ordering and a phase transition due to a reduction of dielectric interfaces perpendicular to $\vec{E}$ is found. At higher electric field strengths, the electroactivity of PFEMS is exploited to induce a morphological transition as the oxidation of the ferrocenyl groups in the PFEMS block increases the PFEMS volume fraction. Furthermore, charging effects are also expected to have an influence on the morphology. This work therefore demonstrates the extensive tunability of the microdomain morphology and orientation of block copolymers with an iron-containing block by annealing in an electric field which could make them useful in nanofabrication or surface patterning applications.

References

1 K. Yamauchi, S. Akasaka, H. Hasegawa, H. Iatrou and N. Hadjichristidis, *Macromolecules*, 2005, **38**, 8022–8027.

2 T. Gemma, A. Hatano and T. Dotera, *Macromolecules*, 2002, **35**, 3225–3237.

3 N. Hadjichristidis, H. Iatrou, S. K. Behal, J. J. Chiudzinski, M. M. Disko, R. T. Garner, K. S. Liang, D. J. Lohse and S. T. Milner, *Macromolecules*, 1993, **26**, 5812–5815.

4 K. Aissou, H. K. Choi, A. Nunns, I. Manners and C. A. Ross, *Nano Lett.*, 2013, **13**, 835–839.

5 K. Hayashida, T. Dotera, A. Takano and Y. Matsushita, *Phys. Rev. Lett.*, 2007, **98**, 195502.

6 K. Hayashida, W. Kawashima, A. Takano, Y. Shinohara, Y. Amemiya, Y. Nozue and Y. Matsushita, *Macromolecules*, 2006, **39**, 4869–4872.

7 K. Yamauchi, K. Takahashi, H. Hasegawa, H. Iatrou, N. Hadjichristidis, T. Kaneko, Y. Nishikawa, H. Jinnai, T. Matsui, H. Nishioka, M. Shimizu and H. Furukawa, *Macromolecules*, 2003, **36**, 6962–6966.

8 T. Dotera and A. Hatano, *J. Chem. Phys.*, 1996, **105**, 8413–8427.

9 A. Takano, S. Wada, S. Sato, T. Araki, K. Hirahara, T. Kazama, S. Kawahara, Y. Isono, A. Ohno, N. Tanaka and Y. Matsushita, *Macromolecules*, 2004, **37**, 9941–9946.

10 S. Sioula, N. Hadjichristidis and E. L. Thomas, *Macromolecules*, 1998, **31**, 5272–5277.

11 S. Sioula, N. Hadjichristidis and E. L. Thomas, *Macromolecules*, 1998, **31**, 8429–8432.

12 J. Zhuo, G. R. Whittell and I. Manners, *Macromolecules*, 2014, **47**, 3529–3543.

13 K. Kulbaba and I. Manners, *Macromol. Rapid Commun.*, 2001, **22**, 711–724.

14 D. A. Foucher, R. Ziembinski, B. Z. Tang, P. M. Macdonald, J. Massey, C. R. Jaeger, G. J. Vancso and I. Manners, *Macromolecules*, 1993, **26**, 2878–2884.

15 J. K. Li, S. Zou, D. A. Rider, I. Manners and G. C. Walker, *Adv. Mater.*, 2008, **20**, 1989–1993.

16 M. Ginzburg, M. J. MacLachlan, S.-M. Yang, N. Coombs, T. W. Coyle, N. P. Raju, J. E. Greedan, R. H. Herber, G. A. Ozin and I. Manners, *J. Am. Chem. Soc.*, 2002, **124**, 2625–2639.

17 R. Rulkens, R. Resendes, A. Verma, I. Manners, K. Murti, E. Fossum, P. Miller and K. Matyjaszewski, *Macromolecules*,

1997, **30**, 8165–8171.
18 L. Bakueva, E. H. Sargent, R. Resendes, A. Bartole and I. Manners, *J. Mater. Sci: Mater. Electron.*, 2001, **12**, 21–25.
19 K. Amundson, E. Helfand, D. D. Davis, X. Quan, S. S. Patel and S. D. Smith, *Macromolecules*, 1991, **24**, 6546–6548.
20 V. Olszowka, M. Hund, V. Kuntermann, S. Scherdel, L. Tsarkova, A. Böker and G. Krausch, *Soft Matter*, 2006, **2**, 1089–1094.
21 V. Olszowka, M. Hund, V. Kuntermann, S. Scherdel, L. Tsarkova and A. Böker, *ACS Nano*, 2009, **3**, 1091–1096.
22 A. Böker, K. Schmidt, A. Knoll, H. Zettl, H. Hänsel, V. Urban, V. Abetz and G. Krausch, *Polymer*, 2006, **47**, 849–857.
23 A. Böker, H. Elbs, H. Hänsel, A. Knoll, S. Ludwigs, H. Zettl, A. V. Zvelindovsky, G. J. A. Sevink, V. Urban, V. Abetz, A. H. E. Müller and G. Krausch, *Macromolecules*, 2003, **36**, 8078–8087.
24 J. Y. Wang, J. M. Leiston-Belanger, J. D. Sievert and T. P. Russell, *Macromolecules*, 2006, **39**, 8487–8491.
25 J.-Y. Wang, T. Xu, J. M. Leiston-Belanger, S. Gupta and T. P. Russell, *Phys. Rev. Lett.*, 2006, **96**, 128301–128304.
26 T. L. Morkved, M. Lu, A. M. Urbas, E. E. Ehrichs, H. M. Jaeger, P. Mansky and T. P. Russell, *Science*, 1996, **273**, 931–933.
27 K. Amundson, E. Helfand, X. Quan and S. D. Smith, *Macromolecules*, 1993, **26**, 2698–2703.
28 K. Amundson, E. Helfand, X. Quan, S. D. Hudson and S. D. Smith, *Macromolecules*, 1994, **27**, 6559–6570.
29 J. J. McDowell, N. S. Zacharia, D. Puzzo, I. Manners and G. A. Ozin, *J. Am. Chem. Soc.*, 2010, **132**, 3236–3237.
30 W. Q. Shi, S. Cui, C. Wang, L. Wang, X. Zhang, X. J. Wang and L. Wang, *Macromolecules*, 2004, **37**, 1839–1842.
31 S. Zou, M. A. Hempenius, H. SchÃűnherr and G. J. Vancso, *Macromol. Rapid Commun.*, 2006, **27**, 103–108.
32 D. A. Rider, K. A. Cavicchi, K. N. Power-Billard, T. P. Russell and I. Manners, *Macromolecules*, 2005, **38**, 6931–6938.
33 A. Nunns, C. A. Ross and I. Manners, *Macromolecules*, 2013, **46**, 2628–2635.
34 Y. Tsori, *Rev. Mod. Phys.*, 2009, **81**, 1471–1494.
35 T. Xu, A. V. Zvelindovsky, G. J. A. Sevink, O. Gang, B. Ocko, Y. Q. Zhu, S. P. Gido and T. P. Russell, *Macromolecules*, 2004, **37**, 6980–6984.
36 M. Peter, M. A. Hempenius, E. S. Kooij, T. A. Jenkins, S. J. Roser, W. Knoll and G. J. Vancso, *Langmuir*, 2004, **20**, 891–897.
37 A. F. M. Barton, *Handbook of Polymer-Liquid Interaction Parameters and Solubility Parameters*, CRC Press, 1990.
38 J. L. Gardon, *Journal of paint technology*, 1966, **38**, 43–57.
39 J.-C. Eloi, D. A. Rider, G. Cambridge, G. R. Whittell, M. A. Winnik and I. Manners, *J. Am. Chem. Soc.*, 2011, **133**, 8903–8913.
40 H. K. Choi, A. Nunns, X. Y. Sun, I. Manners and C. A. Ross, *Advanced Materials*, 2014, **26**, 2474–2479.
41 S. G. J. A. L. Tsarkova and G. Krausch, *G. Krausch*, 2010, vol. 227, pp. 33–73.
42 S. Ludwigs, G. Krausch, R. Magerle, A. V. Zvelindovsky and G. J. A. Sevink, *Macromolecules*, 2005, **38**, 1859–1867.
43 L. Tsarkova, *Macromolecules*, 2012, **50**, 7985–7994.
44 A. Knoll, L. Tsarkova and G. Krausch, *Nano Lett.*, 2007, **7**, 843–846.
45 A. Knoll, A. Horvat, K. S. Lyakhova, G. Krausch, G. J. A. Sevink, A. V. Zvelindovsky and R. Magerle, *Phys. Rev. Lett.*, 2002, **89**, 035501.

Acknowledgement: C.C.K. thanks the Fonds der Chemischen Industrie and the
DAAD (German Academic Exchange Service) for financial support. The authors are grateful to C-SPIN, a STARnet Center of SRC funded by DARPA and MARCO, and to TSMC for supporting this work. Facilities from the NanoStructures Laboratory and the Center for Materials Science and Engineering under NSF award DMR1419807 were used. We are grateful for the advice of James Daley, William Putnam, Adam McCaughan, Christian Lewin, and Ryan O'Keefe.